JMEPEG (2005) 14:173-178
DOI: 10.1361/10599490522374

1059-9495/$19.00

A Three-Component Strain Gage Dynamometer for Grinding and Polishing Force Measurement

C.H. Liu, C.-C.A. Chen, Chia-Yen Lin, and Chia-Jui Lin

(Submitted March 9, 2004)

The design of a strain gage dynamometer to measure three-dimensional grinding forces during surface finishing of molds and dies is presented in this article. The dynamometer is composed of four measuring blocks to which strain gages are attached. The measuring blocks in this study were designed so that when strain gages are attached at particular places, the blocks deform in such a way that forces in the *x*, *y*, and *z* directions can be separated with little interaction. This behavior was confirmed with finite-element results, and static calibrations performed on the measuring blocks further verified this behavior. In this study, the dynamometer is used to measure grinding forces in a surface-finishing system with a hand grinder mounted on a spindle of a machining center.

Keywords: dynamometer, force measurement, grinding, polishing

1. Introduction

Very often, a material removal process is performed together with force measurement. Force measurement is, therefore, a part of the study of material removal processes (Ref 1). Octagonal ring dynamometers have been used and discussed by many researchers (Ref 1-4). In most cases, the octagonal ring dynamometers can measure forces in the normal (or radial) and tangential directions. A variety of modified designs exist, however, to upgrade octagonal rings to measure forces in more than two component directions. In the designs given by Shaw (Ref 1) and Hsu and Choi (Ref 2), the third force component could also be measured because the four octagonal rings were mounted so that they faced in two different but orthogonal directions. Brewer and Hull (Ref 5) proposed a similar design, in which four half-octagonal rings were used and six force components could be measured. Due to interactions, the calibration processes of these designs required the determination of calibration matrices of size 3 × 3 for the design by Hsu and Choi (Ref 2), and 8 × 6 for the design of Brewer and Hull (Ref 5). Zhe-Jun et al. (Ref 6) modified the structure of the octagonal ring, and strain gages were oriented so that bending strains, shear strains, and axial strains could be measured. The dynamometer so designed was able to measure three-component forces. In this article, a new design for a three-component dynamometer with octagonal measuring blocks is presented. In this design, each measuring block can measure three force components, and interactions can be eliminated within each measuring block.

C.H. Liu and **C.-J. Lin,** Department of Mechanical and Electromechanical Engineering, Tamkang University, Tamsui, Taipei Shien, Taiwan, Republic of China 251; **C.-C.A. Chen,** Department of Mechanical Engineering, National Taiwan University of Science and Technology, No. 43, Section 4, Keelung Road, Taipei, Taiwan, Republic of China 106; and **C.-Y. Lin,** TOP Crystal Technology Inc., No.336-2 Chien Kuo Road, Chu Nan Chen, Miaoli Shien, Taiwan, Republic of China. Contact e-mail: l823chia@ms39.hinet.net.

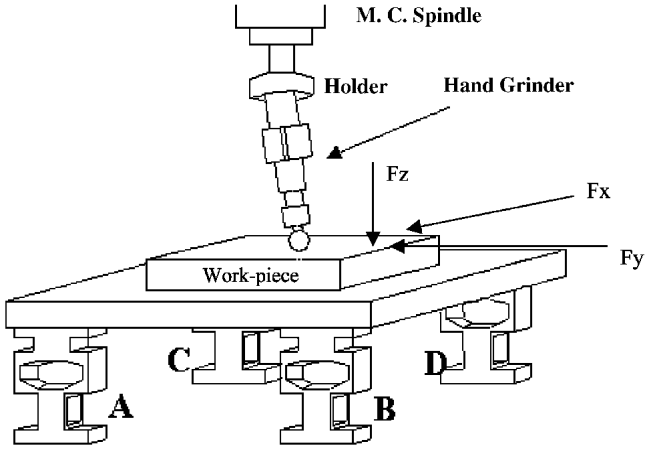

Fig. 1 Dynamometer in an automatic grinding system

2. Construction

The dynamometer shown in Fig. 1 includes four measuring blocks mounted between two plates. The measuring block shown in Fig. 2 contains two orthogonal hollow regions, which can undergo appreciable deformation when loaded by any of the force components (i.e., F_x, F_y, and F_z). Strain gages are attached to each of these measuring blocks at positions of maximum axial strain, ε_{zz} (in absolute values), and these positions may be determined by finite-element (FE) analyses. In this research, the FE software COSMOS-M is used. The mesh contains 4092 quadratic, 10-node, tetrahedral elements and 7677 nodes. As a force $F_x = 100$ N is applied to the top of a measuring block the bottom surface of which is fixed, and the deformed shape (exaggerated) obtained by FE analyses is shown in Fig. 3. Strain gage positions for this force are indicated as X_1 and X_2 (Fig. 2). Similarly, strain gage positions for F_y, and F_z are (Y_1, Y_2) and (Z_1, Z_2), respectively, as Fig. 2 shows.

As the measuring block is subjected to a single force, F_x, on the top surface (i.e., the same loading causes the deformation shown in Fig. 3), FE results show that axial strains ε_{zz} at strain

gage positions X_1 and X_2 have opposite signs. The average strain for block A may be defined as:

$$\varepsilon_A(x) = \frac{1}{2}(\varepsilon_{AX_1} - \varepsilon_{AX_2}) \quad \text{(Eq 1)}$$

where ε_{AX_1} and ε_{AX_2} are strains measured by gages X_1 and X_2 on measuring block A. As strain gages on blocks A, B, C, and D are connected in the way shown in Fig. 4, then the output voltage E_X is given by:

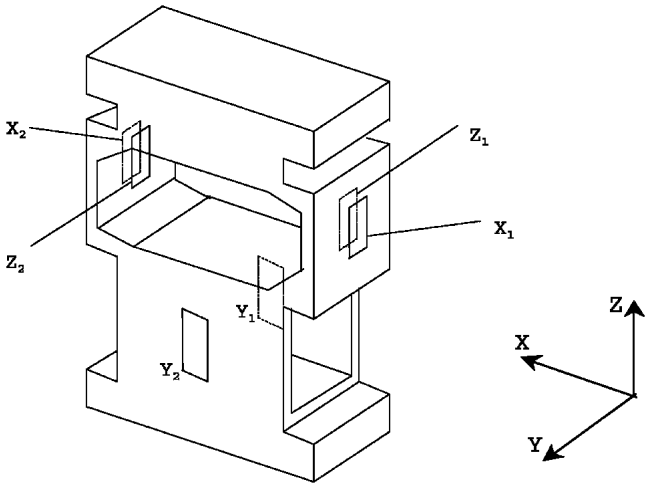

Fig. 2 Strain gage positions on a measuring block

$$E_X = \frac{1}{8}(\varepsilon_{AX_1} - \varepsilon_{AX_2} + \varepsilon_{BX_1} - \varepsilon_{BX_2} + \varepsilon_{CX_1} - \varepsilon_{CX_2} + \varepsilon_{DX_1} - \varepsilon_{DX_2}) \times K \times E \quad \text{(Eq 2)}$$

where K is the gage factor, and E is the voltage. The electric circuit for F_x may be found in Lin (Ref 7). If strain gages Y_1 and Y_2 are used instead of X_1 and X_2, then the force F_y may be measured. The connection of the strain gages onto the four measuring blocks and the electric circuit for F_y are the same as those for F_x (also found in Lin, Ref 7).

Now consider the case in which a force, F_z, is applied to the top surface of measuring block A. It can be seen that if F_z is downward, then $\varepsilon_{zz} < 0$ for strain gages Z_1 and Z_2. Hence, the average strain may be defined as:

$$\varepsilon_A(z) = \frac{1}{2}(\varepsilon_{AZ_1} + \varepsilon_{AZ_2}) \quad \text{(Eq 3)}$$

If strain gages on four measuring blocks are connected in the way shown in Fig. 5, then the output voltage E_Z is given by (Ref 7, 8):

$$E_Z = \frac{1}{8}(\varepsilon_{AZ_1} + \varepsilon_{AZ_2} + \varepsilon_{BZ_1} + \varepsilon_{BZ_2} + \varepsilon_{CZ_1} + \varepsilon_{CZ_2} + \varepsilon_{DZ_1} + \varepsilon_{DZ_2}) \times K \times E \quad \text{(Eq 4)}$$

The electric circuit for measuring F_z may once again be found in Ref 7.

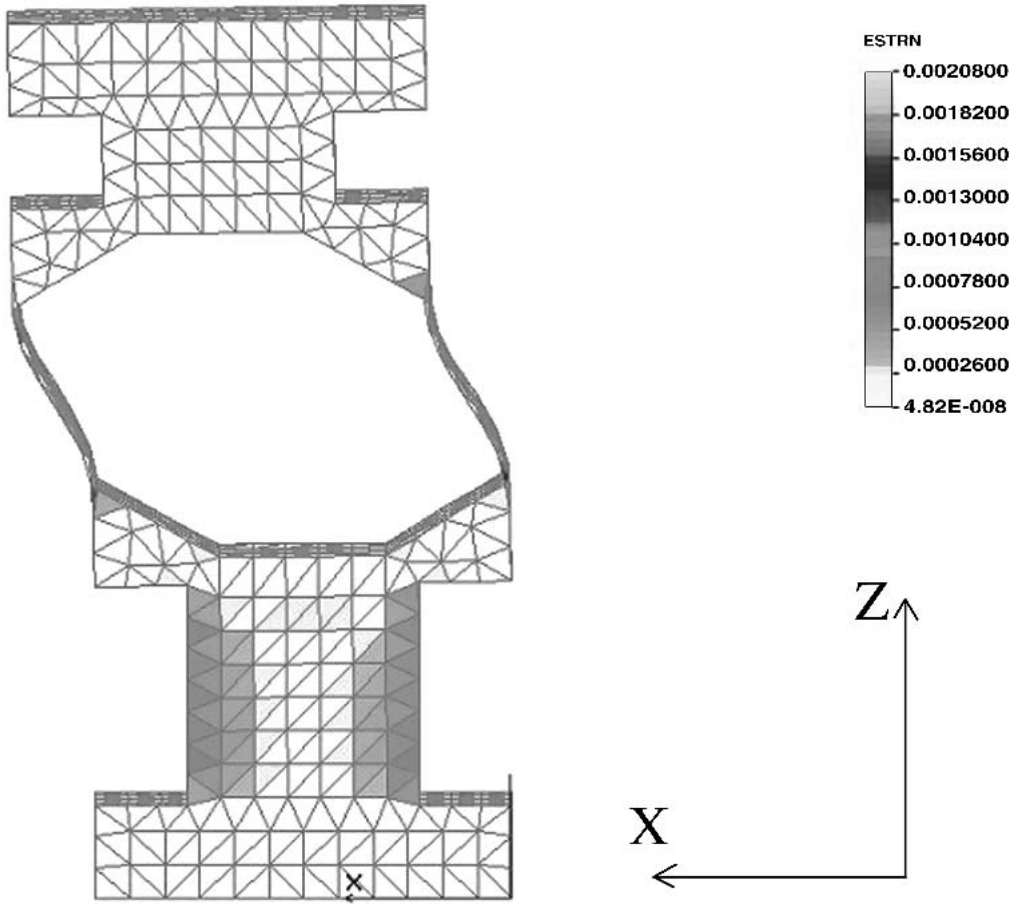

Fig. 3 Deformed shape of the measuring block as a force $F_x = 100$ N is applied

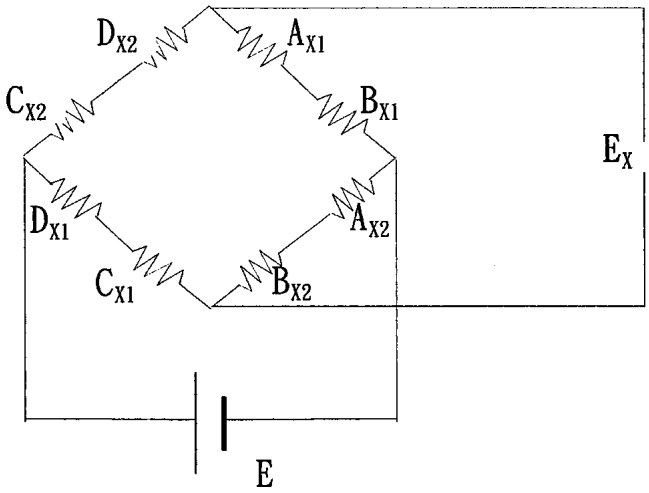

Fig. 4 Connection of strain gages for measuring F_x

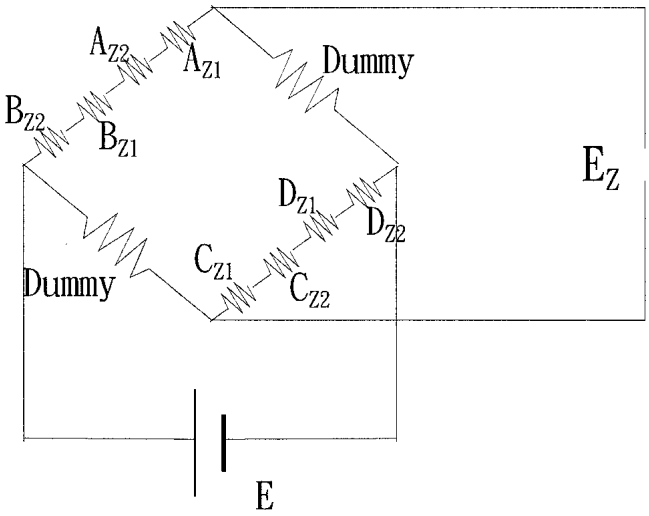

Fig. 5 Connection of strain gages for measuring F_z

3. Elimination of Interactions

Figure 6 shows the top view of the upper plate. Four measuring blocks are fixed to the plate at points *A*, *B*, *C*, and *D*. The workpiece is fixed to the surface of the plate, and, during the grinding process, the resultant contact force between the workpiece and the plate, $\vec{R} = R_x\vec{i} + R_y\vec{j} + R_z\vec{k}$, is applied at point *P*. The coordinates of point *P*, measured from the origin *O*, are given as *x* and *y*, and the moment produced by $\vec{R}$ about the point *A* may be shown to be:

$$\begin{aligned}\vec{M}_A &= M_x\vec{i} + M_y\vec{j} + M_z\vec{k} \\ &= \left(\frac{1}{2}H - y\right)R_z\vec{i} - \left(\frac{1}{2}W - x\right)R_z\vec{j} + \left[\left(\frac{1}{2}W - x\right)R_y \right. \\ &\quad \left. - \left(\frac{1}{2}H - y\right)R_x\right]\vec{k} \end{aligned} \quad \text{(Eq 5)}$$

Hence, this moment is three-dimensional, and each component is generally nonzero. F_x, F_y, and F_z denote forces applied to measuring block *A* (Fig. 7). Because measuring block *A* is bolted to the upper plate at the geometric center of its upper surface, forces F_x, F_y, and F_z, are applied to the measuring block at roughly the center. Due to symmetry, the force F_z causes equal strains in X_1 and X_2, and, from Eq 1, they cancel each other. Therefore, the normal force F_z has little effect on measuring the tangential force F_x. Likewise, F_z also produces equal strains in gages Y_1 and Y_2 and has negligible influence on F_y.

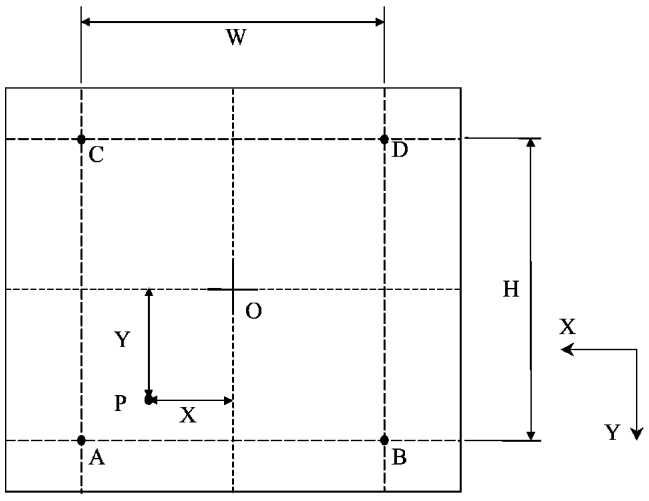

Fig. 6 Top view of the upper plate

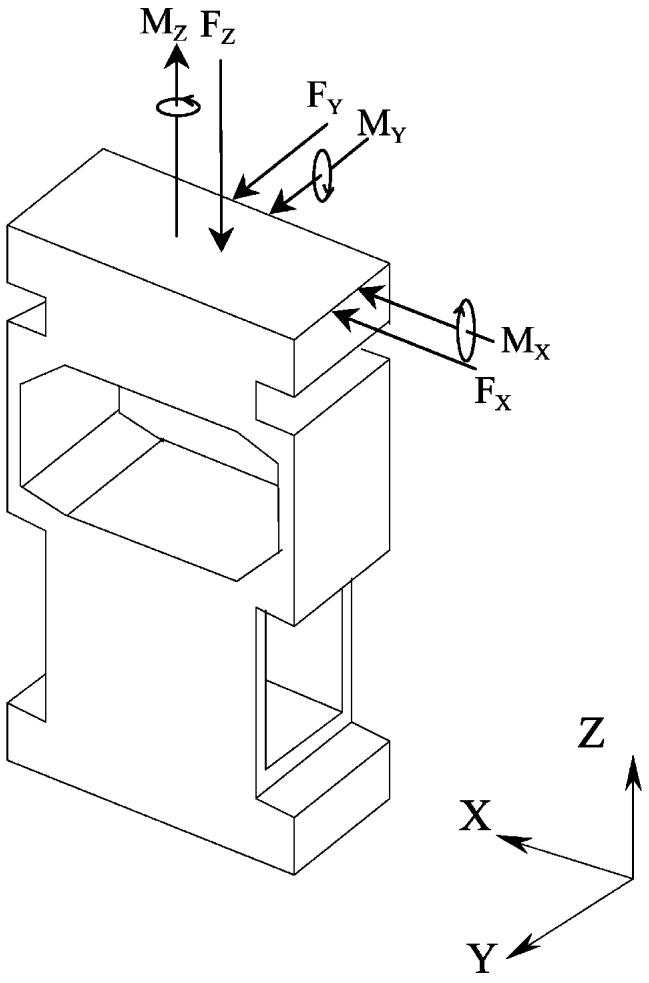

Fig. 7 Forces and moments applied to the measuring block

Table 1 Stresses and strains as the measuring block is subjected to the following forces: (a) F_x = 100 N (b) F_x = 100 N and M_y = 20 N · m

Strain gages	Gage coordinates (x,y,z), cm	FEM nodal coordinates (x,y,z), cm	σ_{xx}, MPa		σ_{yy}, MPa		σ_{zz}, MPa	
			(a)	(b)	(a)	(b)	(a)	(b)
X_1	(0, 0.75, 4.95)	(0, 0.75, 5.03)	−12.51	−12.51	48.42	48.42	186.5	186.5
X_2	(0.05, 0.75, 4.95)	(0.05, 0.78, 4.85)	10.32	10.32	−73.84	−73.84	−246.8	−246.8

Note: FEM, finite-element method

Table 2 Stresses and strains as the measuring block is subjected to the following forces: (a) F_y = 100 N (b) F_y = 100 N and M_x = 20 N · m

Strain gages	Gage coordinates (x,y,z), cm	FEM nodal coordinates (x,y,z), cm	σ_{xx}, MPa		σ_{yy}, MPa		σ_{zz}, MPa	
			(a)	(b)	(a)	(b)	(a)	(b)
Y_1	(2.25, 0, 1.7)	(2.25, 0, 1.63)	67.3	67.3	9.27	9.27	238.1	238.1
Y_2	(2.25, 1.5, 1.7)	(2.32, 1.5, 1.66)	−61.7	−61.7	−6.66	−6.66	−214.5	−214.5

Table 3 Output voltage due to F_x

Loading				Unloading			
	Voltage, V				Voltage, V		
F_x (N)	x-axis	y-axis	z-axis	F_x (N)	x-axis	y-axis	z-axis
0	0	0	0	0	0	0	0
10.0	1.618	0.022	0.044	10.0	1.676	0.024	0.020
20.0	3.312	0.042	0.112	20.0	3.358	0.052	0.044
30.0	4.960	0.068	0.166	30.0	5.004	0.064	0.154
40.0	6.620	0.076	0.260	40.0	6.676	0.082	0.244
50.0	8.300	0.096	0.320	50.0	8.300	0.096	0.320

Next, consider the effect produced by the moment M_y, given by Eq 5, on force F_x. The thin walls on which strain gages X_1 and X_2 are attached (Fig. 2) have very low stiffness, making adjacent parts resemble rigid bodies. Thus, each of these walls may be represented by a beam that is completely fixed at both ends. It may be shown, by using elementary strength of materials, that the couple M_y produces no deformation on a beam that is completely fixed at both ends. Therefore, the moment M_y causes small strains on strain gage positions X_1 and X_2. Similar arguments lead to the conclusion that the moment M_x has little effect on strain gages Y_1 and Y_2.

FE analyses were performed to verify the conclusions reached so far. The same mesh shown in Fig. 3 was used in these analyses. Table 1 shows the results for two loading cases: (a) A force $F_x = 100$ N is applied to the geometric center of the upper surface of the block, and (b) a force $F_x = 100$ N and a couple $M_y = 20$ N · m is also applied to the block. The bottom surface is completely fixed. FE nodal coordinates are determined by the preprocessor and generally do not coincide with strain gage coordinates (shown in the second column in Table 1). The closest nodes (i.e., coordinates shown in the third column) are used for comparison. Normal stresses at these nodes are identical for loading cases a and b. Hence, the moment M_y does not have any influence on stresses produced by the force F_x. Because normal strains may be uniquely determined by these stresses, M_y produces no strains on strain gages X_1 and X_2. Table 2 shows that the stresses in strain gage positions Y_1 and Y_2 are not affected by the moment M_x.

4. Calibration

Static calibrations are performed to verify the analyses discussed above. Balancing weights are imposed and removed from the dynamometer to produce loading and unloading paths. Table 3 and Fig. 8 show output voltages due to force F_x. Note that in Fig. 8 all loading paths coincide with the corresponding unloading path. Results for F_y and F_z are shown in Fig. 9 and 10, respectively, and numerical values are given in Tables 4 and 5, respectively. It can be seen from these figures that little interaction occurs.

5. Measuring Results and Discussions

Rotary hand grinders have become important tools for the grinding and mechanical polishing of molds and dies. They are used for manual operations and also in automatic surface-finishing systems (Ref 9, 10). In a surface-finishing process using a rotary hand grinder with a carbide bur, grinding and polishing forces are generally three-dimensional, and the magnitude of each force component is less than 50 N. This dynamometer is used to the measure grinding forces of a hand grinder driven by a machining center (see Fig. 1) to move along a reciprocal path. Figure 11 shows the measuring results as the hand grinder is driven with a feed rate 25 mm/min while rotating at 10,000 rpm. The grinding depth is 50 μm. The diameter of the tool is 0.3 mm, and the specimen material is S45C steel. It may be seen from these figures that the normal grinding force (F_z) is higher than the tangential forces F_x and F_y and is generally within a range, under the current grinding conditions, of 0 to 6 N. Average grinding forces in the x, y, and z directions are calculated to be 0.23, 0.61, and 2.18 N, respectively. Grinding forces may go up as the hand grinder changes directions along its reciprocal path. At these locations, the normal grinding force (F_z) may reach a value of 9.8 N, or 4.5 times higher than its average value.

6. Conclusions

The measuring block and corresponding strain gage positions proposed in this article may eliminate interactions among

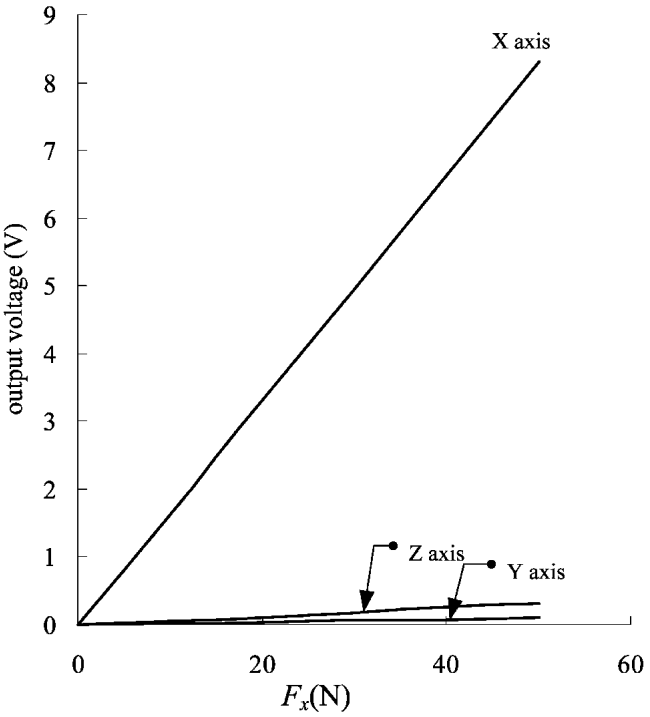

Fig. 8 Calibration curves for F_x

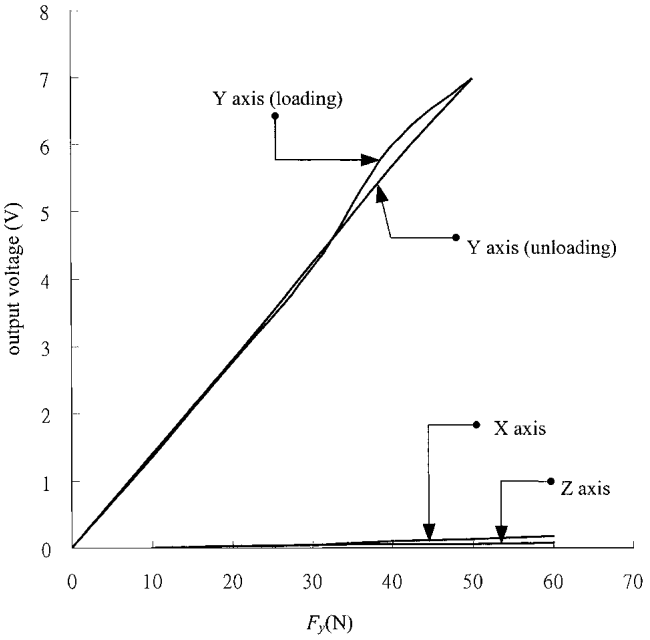

Fig. 9 Calibration curves for F_y

force components. Specifically, the influences of F_z on measuring F_x and F_y are reduced by the symmetry of the block about the xz and the yz planes. Also, interactions between F_x and M_y, and between F_y and M_x, are restrained by fixed-end effects. Calibration results show that the dynamometer constructed with these measuring blocks has little interaction and, hence, may be used for three-dimensional force measurement. This dynamometer was then used to measure the grinding forces of an electric hand grinder driven by a machine center. Along a reciprocal grinding path, the local maxima of the normal grinding force occur at locations where the hand grinder changes direction, and the global maximum force may reach a value 4.5 times higher than the average force.

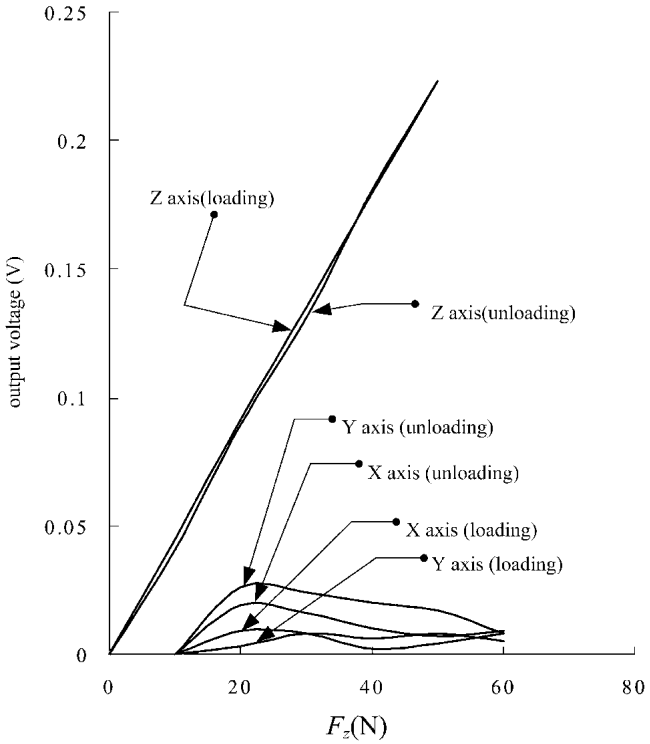

Fig. 10 Calibration curves for F_z

Table 4 Output voltage due to F_y

Loading				Unloading			
	Voltage, V				Voltage, V		
F_y (N)	*x*-axis	*y*-axis	*z*-axis	F_y (N)	*x*-axis	*y*-axis	*z*-axis
0	0	0	0	0	0	0	0
10.0	0.030	1.358	0.028	10.0	0.036	1.398	0.114
20.0	0.046	2.760	0.050	20.0	0.078	2.798	0.080
30.0	0.102	4.156	0.054	30.0	0.104	4.230	0.090
40.0	0.130	5.970	0.058	40.0	0.122	5.662	0.084
50.0	0.170	6.978	0.070	50.0	0.170	6.978	0.070

Table 5 Output voltage due to F_z

Loading				Unloading			
	Voltage, V				Voltage, V		
F_z (N)	*x*-axis	*y*-axis	*z*-axis	F_z (N)	*x*-axis	*y*-axis	*z*-axis
0	0	0	0	0	0	0	0
10.0	0.009	0.003	0.045	10.0	0.019	0.026	0.041
20.0	0.008	0.008	0.091	20.0	0.016	0.024	0.089
30.0	0.002	0.006	0.135	30.0	0.010	0.020	0.131
40.0	0.004	0.008	0.180	40.0	0.007	0.017	0.181
50.0	0.008	0.005	0.223	50.0	0.009	0.008	0.223

Acknowledgment

The authors gratefully acknowledge the support given by the National Science Council of the Republic of China under grant No. NSC 87-2212-E032-002.

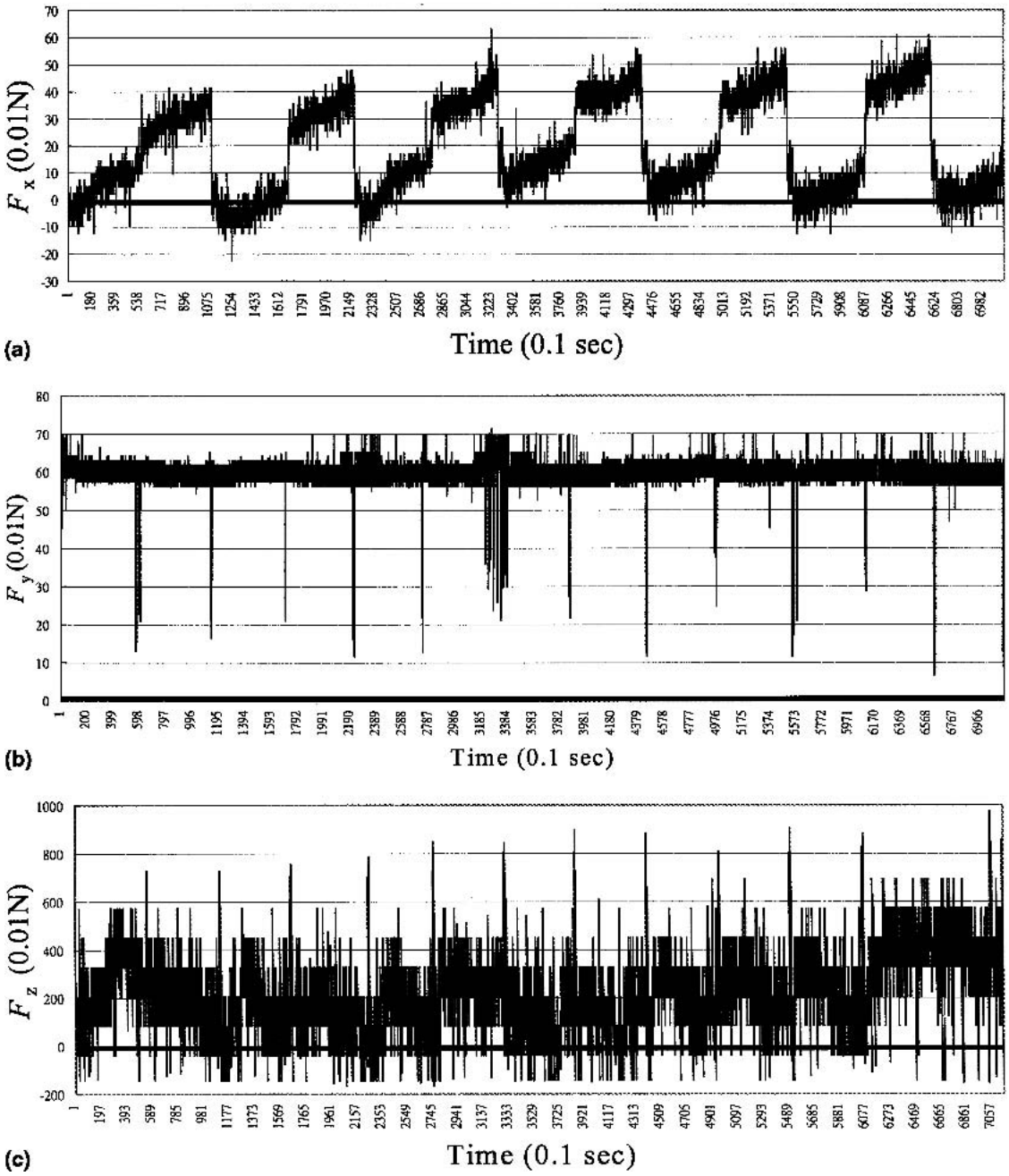

Fig. 11 Measuring results of grinding forces. (a) Force F_x. (b) Force F_y. and (c) Force F_z

References

1. M.C. Shaw, *Metal Cutting Principles,* Oxford University Press, 1984
2. T.C. Hsu and C.Y. Choi, Measurement and Representation of Cutting Force Due to Oblique Machining, *Int. J. Machine Tool Design Res.,* Vol 10, 1970, p 49-64
3. R.J. Godwin, An Extended Octagonal Ring Transducer for Use in Tillage Studies, *J. Agric. Eng.,* Vol 20, 1975, p 346-352
4. S. Majumdar, E.V. Thomas, and D.S. Jayas, Optimization of Parameters in the Design of an Extended Octagon-Ring Transducer, *Agric. Eng. J.,* Vol 3, 1994, p 152-165
5. R.M. Brewer and M.L. Hull, The Effect of Interface Plate Compliance on Dynamometers Incorporating Octagonal Strain Rings, *Exp. Mech.,* Vol 35 (No. 4), 1995, p 337-344
6. Y. Zhe-Jun, C. Li-Jun, and Z. Pan, "A New Type of Three-Component Dynamometer with High Stiffness and High Natural Frequency," Proceedings of 26th International M.T.D.R. Conference, B.J. Davis, Ed., Palgrave Macmillan Press, 1987, p 313-316
7. C.Y. Lin, "Three Dimensional Grinding Force Measurement in Mold Grinding Process," Master's thesis, Tamkang University, 1999 (in Chinese)
8. C.J. Lin, "Contact Force Measurement in Mold Grinding Process," Master's thesis, Tamkang University, 1997 (in Chinese)
9. C.A. Chen and N.A. Duffie, Development of an Automatic Surface Finishing System (ASFS) with In-Process Surface Topography Inspection, *J. Mater. Proc. Technol.,* Vol 62 (No. 4), 1996, p 427-430
10. T.C. Hsu, "Automatic Surface Finishing with Rough Area Pattern Recognition," Ph.D. dissertation, University of Wisconsin-Madison, 1998